Analyst

PAPER

View Article Online
View Journal

Cite this: DOI: 10.1039/d6an00255b

Quantitative analysis of colorimetric hydrogel/paper mini-disk arrays using a handheld Wi-Fi scanner

Lin Qi,†[a] Pitipat Parittothok,†[a,b] Sophia Sun,[a] Jakrapop Wongwiwat,[b] Aluck Thipayarat,[c] Wanida Laiwattanapaisal [d] and Hua-Zhong Yu *[a,d]

Received 7th March 2026,
Accepted 20th March 2026

DOI: 10.1039/d6an00255b

rsc.li/analyst

Traditional quantitative colorimetric assays often rely on bulky laboratory instruments, such as UV-vis spectrophotometers and microplate readers. While smartphone-based point-of-need (PON) tools have emerged as alternatives, they are frequently limited by variation in ambient lighting and perspective distortion. To address these challenges, we developed a PON quantitative platform for colorimetric assays that integrates hydrogel (agarose based) coated filter paper as reaction "mini-disks", a handheld Wi-Fi scanner as the imaging tool, and a custom-designed app (universal for both smartphones and pads) for color analysis. Using two representative colorimetric assays, pH-differential colorimetric assay for anthocyanin and Ellman's assay for parathion methyl, we validated the performance of this new Wi-Fi scanning platform using conventional UV-vis spectrophotometry analysis. The results demonstrate that this integrated Wi-Fi scanning protocol promises a reliable, universal, low-cost, and convenient tool for on-site, quantitative colorimetric analysis in resource-limited settings.

1. Introduction

Colorimetric assays are widely employed analytical techniques that detect target analytes *via* measurable changes in color. These changes typically arise from chemical or enzymatic reactions that convert a reactant or substrate into a chromogenic product with distinct colors.[1–4] In addition, nanomaterials such as gold and silver nanoparticles can serve as colorimetric reagents, which exhibit aggregation-dependent color changes in response to analyte interaction.[5–8] Colorimetric assays can achieve high sensitivity when UV–vis spectrophotometers are used as detectors; meanwhile, they offer distinct advantages over other instrumental techniques (*e.g.*, gas/liquid chromatography and mass spectrometry), such as rapid response, ease of use, and high-throughput.[1,3,7,9] Furthermore, their integration with biosensing strategies, such as the use of chromogenic labels conjugated to biorecognition elements (*e.g.*, antibodies, DNA) has enabled diverse applications in clinical diagnostics, food safety monitoring, and environmental analysis.[3,8,9]

As visible colors generated in colorimetric assays enable direct readout by the naked eye, they facilitate simple qualitative or semi-quantitative detection (*e.g.*, through comparison with a reference color chart) without the need for any instruments or apparatus.[10] A well-established commercial example is the lateral flow immunochromatographic testing strip (*e.g.*, pregnancy tests), in which the appearance of a colored band in the test region indicates the presence of the target analyte.[11,12] For quantitative analysis, UV-vis absorbance measurements of the chromogenic products remain as the conventional method. According to Beer's law, the absorbance of a colored compound is directly proportional to its concentration in solution. In practice, this involves the identification of the maximum absorption wavelength from the scanned spectrum, followed by the determination of absorbance values for a series of standard solutions with known analyte concentrations. A calibration curve is then constructed, enabling the determination of analyte concentrations in unknown samples by interpolation.[4,13,14]

In recent years, smartphones with high-resolution cameras and fast data processing hardware have emerged as powerful platforms for quantitative colorimetric assays, and their integration enables on-site, point-of-need (PON), and real-time analysis in diverse settings, including households, clinics, and in-field environments.[15–24] Using this tool, assay results are

[a]Department of Chemistry, Simon Fraser University, Burnaby, British Columbia V5A 1S6, Canada. E-mail: hogan_yu@sfu.ca
[b]Department of Mechanical Engineering, King Mongkut's University of Technology Thonburi, Bangkok 10140, Thailand
[c]Department of Food Engineering, King Mongkut's University of Technology Thonburi, Bangkok 10140, Thailand
[d]Department of Clinical Chemistry, Chulalongkorn University, Bangkok 10330, Thailand
† These authors contributed equally to this work.

captured as digital images, which can then be processed using commercial software (*e.g.*, Photoshop, ImageJ) or customized apps.[15,17,25,26] Color information is analyzed in grayscale or various color spaces (*e.g.*, RGB or CMYK), and quantitative results are obtained by correlating the color intensity with the analyte concentration.[19,21,24] Moreover, with internet and cloud-based information systems, smartphones allow easy data management, storage, remote access, sharing and delivery for further analysis. Besides smartphones, flatbed scanners have been explored as alternative imaging tools for colorimetric assays; particularly handheld portable scanners offer advantages of low cost (CAD 100–500 depending on the exact model/brand and supplier), on-site use, and wireless connection (*e.g.*, Wi-Fi, Bluetooth) with smartphones, laptops, and other electronic devices for data transfer and analysis.[27]

With the increasing adoption of smartphones and scanners as imaging tools for colorimetric assays, the devices to run such assay reactions have also evolved to be adaptable for PON testing. For example, filter paper is a popular substrate material that has been extensively explored for preparing colorimetric assays, as it is inexpensive, biocompatible, and easy to handle.[10,28–31] Moreover, the highly porous and hydrophilic structure (a network of cross-linked cellulose fibers) of filter paper provides high permeability and strong capillary function, which enables spontaneous fluid flow without the need for external pumping.[10,28,31] Such a porous structure also allows for the preloading of reagents into filter paper and thereby simplifies the detection process.[29] With wax printing, hydrophobic coatings, and UV lithography (with a patterned mask), reaction channels of specific dimensions and shapes can be created on filter paper.[26,29,32–34] Furthermore, the abundant functional groups of cellulose fibers (*e.g.*, hydroxyl moieties) allow for diverse chemical and biological modifications, which significantly broadens the application scope of filter paper-based analytical devices.[35] Besides filter paper, hydrogels with a water-swollen 3D polymer network structure have distinctive physical, chemical, mechanical and biological properties, which have also demonstrated similar advantages as the substrate for colorimetric assays.[36,37] We and others have recently developed novel pH testing strips by coating filter paper with an agarose-based hydrogel, which results in enhanced loading capability and uniformity of chromogenic reagents (minimized "coffee-ring" effect), as well as improved color retention for quantitative analysis.[34,38]

In the present work, we explore the feasibility of creating an array of hydrogel-coated paper mini-disks, which would allow multiplex PON colorimetric detection, in conjunction with Wi-Fi scanning for data analysis. Specifically, the images of detection results are captured using a handheld Wi-Fi scanner, and the quantitation is performed *via* a customized app capable of analyzing color information in different color spaces (*e.g.*, RGB, CMYK). To validate this new platform as a PON quantitative tool for colorimetric assays, we examined two diverse analytes (anthocyanin and parathion methyl) and compared their detection results to those obtained from conventional spectrophotometry measurements.

2. Results and discussion

2.1. Fabrication of hydrogel-paper mini-disk arrays for colorimetric assays

Hydrogel (agarose-based) coated filter paper was fabricated by modifying a simple procedure reported in our previous work;[34] the details are provided in the Experimental section. In contrast to the previous work, where agarose solution was mixed with colorimetric reagents (*i.e.*, anthocyanin as a pH indicator) before coating, herein pure agarose solutions are used and the coated filter paper can be loaded with any colorimetric reagents depending on specific needs. As shown in Fig. 1A, the detection arrays are readily prepared by machine-cutting the coated filter paper into mini-disks (5 mm diameter), which are well-aligned and assembled onto a double-sided tape. Since the tape is hydrophobic (water contact angle = 99 ± 2°), droplets of aqueous solutions (as much as 30 μL) can be held well by the agarose-paper disk, which is easily adjusted by varying its diameter or even the shape.

To obtain the image of testing results, the mini-disk array is placed in an "imaging box" (3D-printed or using a stack of cardboard with a rectangular opening in the center). A handheld Wi-Fi scanner (iScan) is used to capture the image (1050 dpi) by moving it across the disk arrays (the built-in feedback mechanism of iScan scanners ensures the proper scanning speed of 2.5–3.0 cm s^{-1} for the selected resolution).[39] If the speed is too slow or too fast, warning symbols will appear on the device and the scan will stop automatically. The thickness of the imaging box (~2.5 mm) ensures that the bottom of the scanner (sensing area) does not touch the hydrogel-paper disks. After scanning, the image is automatically saved, which can be transferred to a smartphone or a pad *via* Wi-Fi. To analyze the color information, a custom-designed app (ChromaDetect) was used, which can run on any device (smartphones, pads, or laptops) with a web browser (no OS restrictions) and supports uploading images in either PNG or JPEG format. With one or multiple pre-defined areas (a circle or rectangular region with adjustable coordinates and dimensions), the app is able to analyze the color information (based on either the RGB or CMYK color space) for each pixel and provide average and standard deviation values as outputs. In addition, a linear calibration equation (with fitted slope and intercept values) can be created, which enables the calculation of analyte concentration based on normalized color intensity. The results determined using this app can be exported to Excel sheets (xlsx) for further analysis if preferred. The original code of this app and the screenshot of its interface are provided in the SI.

2.2. Wi-Fi scanning pH-differential colorimetric assay for the quantitation of anthocyanins

We first validated this new analytical platform with a pH-differential colorimetric assay for anthocyanins (a class of water-soluble natural pigment that is widely used in the food industry and has important nutritional value as antioxidants).[39,40] Developed by Sondheimer and Kertesz in 1948 and officially

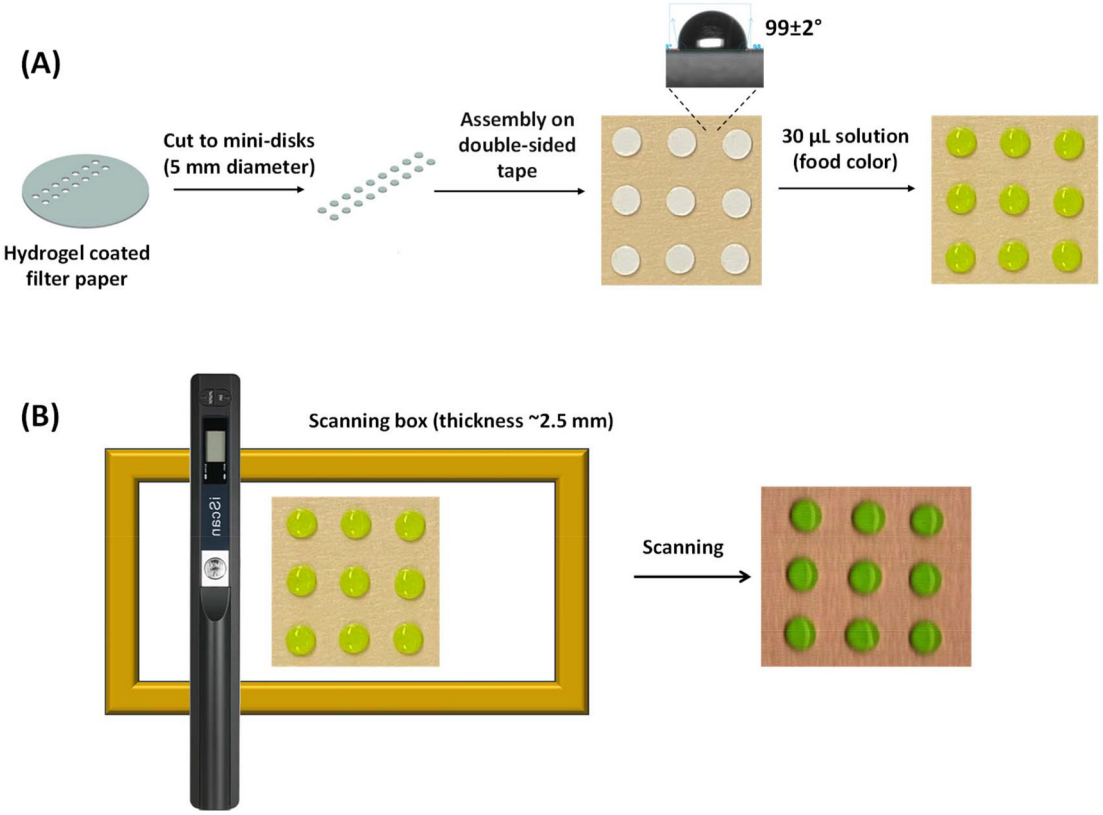

Fig. 1 (A) Cutting and assembling of hydrogel/paper mini-disk arrays. (B) Imaging the detection results by using a handheld Wi-Fi scanner (iScan).

adopted by the Association of Official Agricultural Chemists (AOAC) since 2005,[41,42] the pH differential colorimetric assay we have performed is the standard protocol for monitoring anthocyanin levels in agricultural products. The major species of anthocyanin, cyanidin-3-*O*-glucoside (>50%), was particularly used in this study as the standard analyte for the quantitative detection as described below.

The principle of this pH-differential colorimetric assay is based on the structural switch of anthocyanin (Cy3G) from a red-colored flavylium cation in a pH < 2 environment to a pair of colorless, resonant structures (hemiketal and chalcone) at pH 4–5 *via* hydration and deprotonation processes (Fig. 2A); with such a differential approach (instead of monitoring color change at a single pH) the matrix effect can be minimized.[42] As such, we have first confirmed the sensing principle by recording the UV/vis spectra for different concentrations of anthocyanin (Cy3G) dissolved in pH 1.0 solution (0.1 M HCl) and pH 4.5 buffer (NaAc/HAc). As shown in Fig. 2B and C, strong absorbance peaks are observed at pH 1.0, which correspond to the fully delocalized π-conjugation of flavylium cations; in contrast, much weaker absorbance was observed at pH 4.5. For example, the absorbance with a concentration of 80 mg L^{-1} is less than 0.1, which is over 1.5 at pH 1.0. This is the result of the disrupted π-conjugation due to the hydration and deprotonation processes (Fig. 2A).

In accordance with a previously reported protocol,[42] an anthocyanin (Cy3G) calibration curve can be established by plotting the difference in the maximum absorbance (ΔA) at 520 nm between pH 1.0 and pH 4.5 as a function of its concentration (*i.e.*, $\Delta A = A_{\mathrm{pH\ 1.0}} - A_{\mathrm{pH\ 4.5}}$). As shown in Fig. 2D, ΔA initially increases with increasing concentrations of anthocyanin (Cy3G), which becomes saturated over 100 mg L^{-1}. Indeed, a linear relationship can be established from 0 to 30 mg L^{-1} with R^2 = 0.9844 (Fig. 2E). Based on the best fitting equation, ΔA = 0.036 ± 0.003 [Cy3G] + 0.011 ± 0.009, the limit of detection (LOD), 0.75 ± 0.06 mg L^{-1} was determined from the slope (k) and the standard deviation (S_b) of the intercept ($3S_b/k$).

As illustrated in Fig. 3, to perform the anthocyanin colorimetric assay on hydrogel/paper disks, each disk was pre-loaded with 20 μL of pH 1.0 solution or pH 4.5 buffer. Afterwards, 20 μL of Cy3G solution of different concentrations was added to each paper disk, followed by scanning with the Wi-Fi scanner to obtain the results right away (as the color appears immediately).

Fig. 4A shows a scanned image of the anthocyanin detection results on two rows of hydrogel/paper disks; it can be seen that with increasing concentrations of anthocyanin, the two rows of paper disks displayed varied colors: the top row (pre-loaded with pH 1.0 solution) changed from plain gray to bright red, while much less color change was observed in the bottom row (pre-loaded with pH 4.5 buffer). By using the developed ChromaDetect app, the color generated on each paper disk was analyzed with the RGB (red, green, and blue)

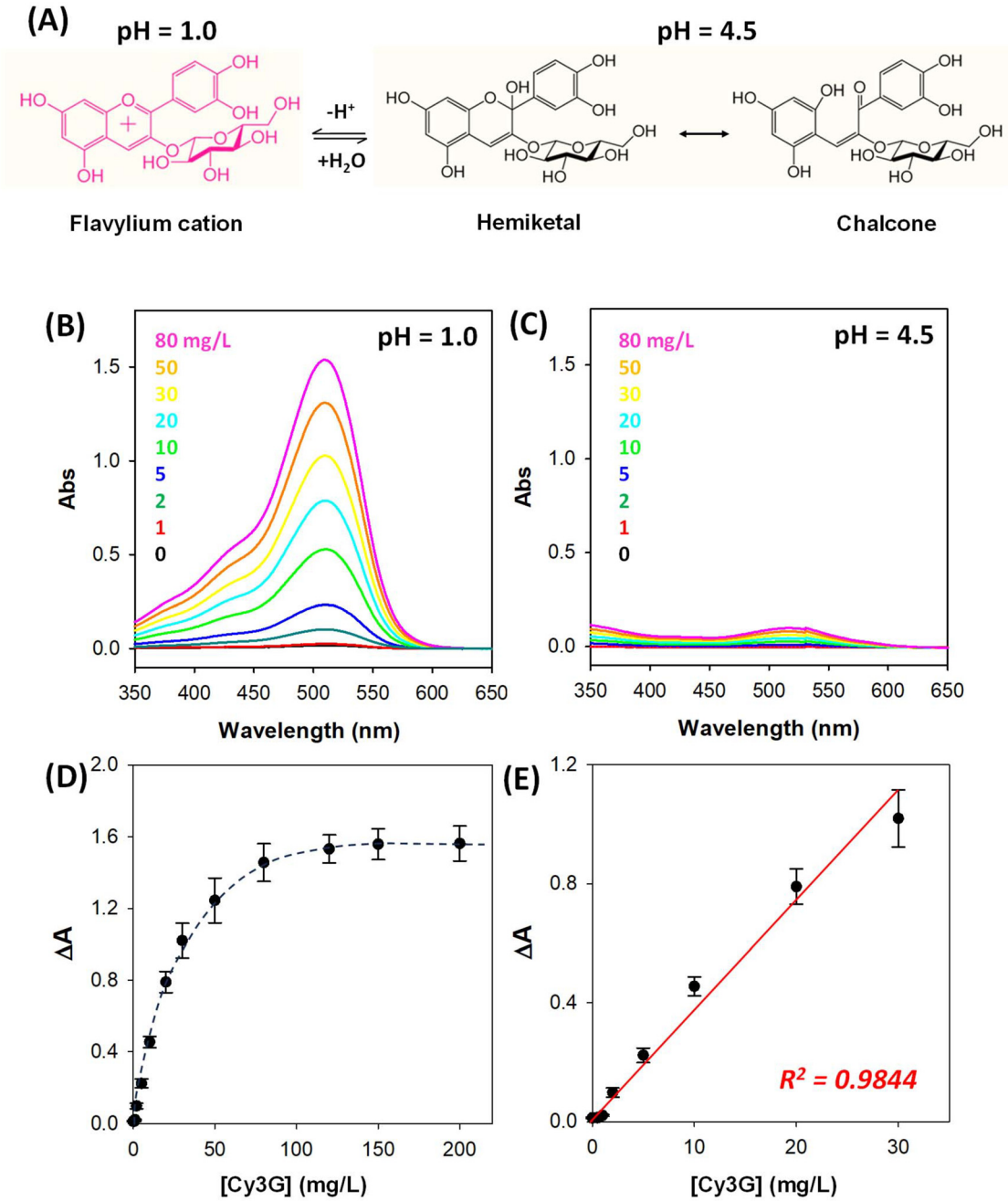

Fig. 2 (A) pH-Dependent structural switching of anthocyanin (Cy3G). UV-vis spectra of different concentrations of anthocyanin (Cy3G) in (B) pH 1.0 solution and (C) pH 4.5 buffer. (D) Anthocyanin (Cy3G) calibration curve obtained using the pH differential colorimetric assay ($\Delta A = A_{\text{pH 1.0}} - A_{\text{pH 4.5}}$). The dashed line is to guide the eyes only. (E) Calibration curve from 0 to 30 mg L^{-1} (red line: the best linear fit). The error bars in (D) and (E) were obtained from at least three repeated experiments.

color space, and the difference in the normalized red color intensity ($\Delta R/\sum$RGB, $\sum$RGB = R + G + B) obtained at pH 1.0 and pH 4.5 ($R/\sum$RGB values at pH 1.0 and pH 4.5 are provided in the SI, Fig. S4) is plotted against the concentration of anthocyanin. From the calibration curve, a bigger difference in $\Delta R/\sum$RGB was observed with increasing concentrations of the anthocyanin (Cy3G) standard, which essentially becomes saturated over 80 mg L^{-1} (Fig. 4B). In Fig. 4C, we have shown the best linear fit to the experimental data in the range of 0 to 30 mg L^{-1}, which yields an equation as: $\Delta R/\sum$RGB = 0.012 ± 0.002[Cy3G] + 0.0015 ± 0.0033, R^2 = 0.9879. The determined LOD (0.82 ± 0.11 mg L^{-1}) is indeed comparable to that of standard spectrophotometric results as described above. It is important to note that the sensing performance of the Wi-Fi scanning method does meet the industrial needs for food and beverage quality control (0.3–3 mg L^{-1}).[43]

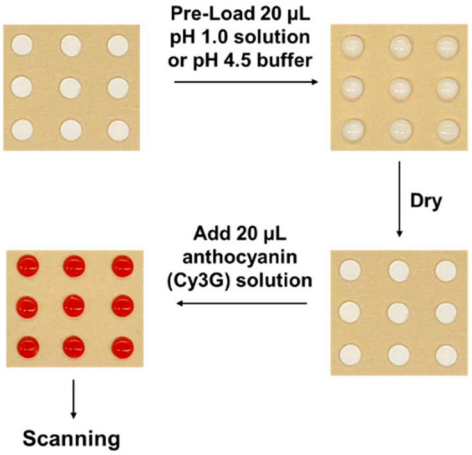

Fig. 3 Performing pH-differential colorimetric assay of anthocyanin (Cy3G) on a hydrogel-paper disk array.

To further evaluate the practical application, we used the above two methods to determine the concentration of anthocyanins in several beverages, which included four raw grape juices and five fermented wines (all samples were obtained from the production line of the Bayou Brewing Club, a sub-division of Laca Biotech Inc., Richmond, BC, Canada). The samples were diluted before testing. Based on their detection signals (ΔA at 512 nm or ΔR/RGB) and the linear calibration curves shown in Fig. 2D and C, the concentrations of anthocyanins in these samples were interpolated and are summarized in Fig. 5A. It is evident that for most samples the quantitation results obtained using the two methods (gray bar: hydrogel/paper disk + Wi-Fi scanning; black bar: UV-vis absorbance measurements) are very close (within experimental uncertainties that were obtained from three repeating tests). For a more direct comparison, the determined concentrations of all samples ($[\text{anthocyanins}]_{\text{scanning}}$ *vs.* $[\text{anthocyanins}]_{\text{abs}}$) are plotted in Fig. 5B; the satisfactory linearity (R^2 = 0.9786) and close-to-unity slope (0.951) of the regression line further confirm the consistency between the conventional UV-vis spectrophotometry and our newly developed Wi-Fi scanning method.

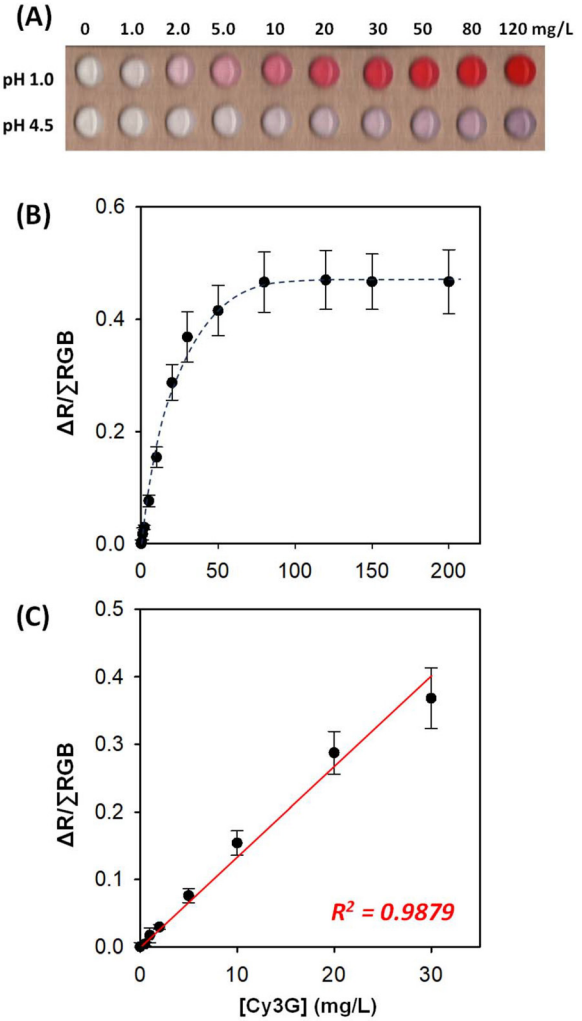

Fig. 4 (A) Scanned image of pH-differential colorimetric assay disks for the anthocyanin quantitation with the corresponding concentration listed on top. (B) Differential red intensities ($\Delta R/\sum\text{RGB} = R/\sum\text{RGB}_{\text{pH 1.0}} - R/\sum\text{RGB}_{\text{pH 4.5}}$) as a function of the Cy3G concentration. The dashed line is to guide the eyes only. (C) Linear calibration data from 0 to 30 mg L^{-1} (red line: the best linear fit). The error bars in (B) and (C) were obtained from at least three repeated experiments.

2.3. Wi-Fi scanning Ellman's assay for the quantitation of parathion-methyl

Parathion methyl is a highly toxic organophosphorus pesticide widely used in agricultural activities, and its detection is critically important due to its severe health risks and environmental persistence. Monitoring of parathion methyl levels in food, water, and soil is essential to prevent acute poisoning, chronic exposure, and ecological damage.[44,45] The gold standard method for detecting parathion methyl is GC-MS, which provides high sensitivity (low μg L^{-1} for water samples and μg kg^{-1} for food and soil), selectivity, and reliable quantification of trace amounts in complex matrices.[46] Although less sensitive than GC-MS, the colorimetric detection of parathion methyl based on Ellman's assay is simple, rapid, and inexpensive; moreover, it can be performed without extensive sample pretreatment, making it a useful tool for high-throughput screening and on-site detection.[47,48] As illustrated in Fig. 6A, the principle of Ellman's assay is to measure the inhibition effect of parathion methyl on the activity of acetylcholinesterase (ATChE). In this assay, the enzyme (ATChE) catalyzes the hydrolysis of acetylthiocholine (ATCh) under slightly alkaline conditions (pH = 7.5–8.0) to produce thiocholine (TCh), which reacts with Ellman's reagent, 5,5′-dithiobis-(2-nitrobenzoic acid) (DTNB), to form a yellow product (TNB) with the peak absorbance at 412 nm. Thus, the decreased color intensity or absorbance indicates the presence of parathion methyl that inhibits the enzymatic activity of ATChE.

To start, we recorded the UV-vis spectra of Ellman's assay solutions with and without adding parathion-methyl. As shown in Fig. 6(B), the standard Ellman's assay (containing

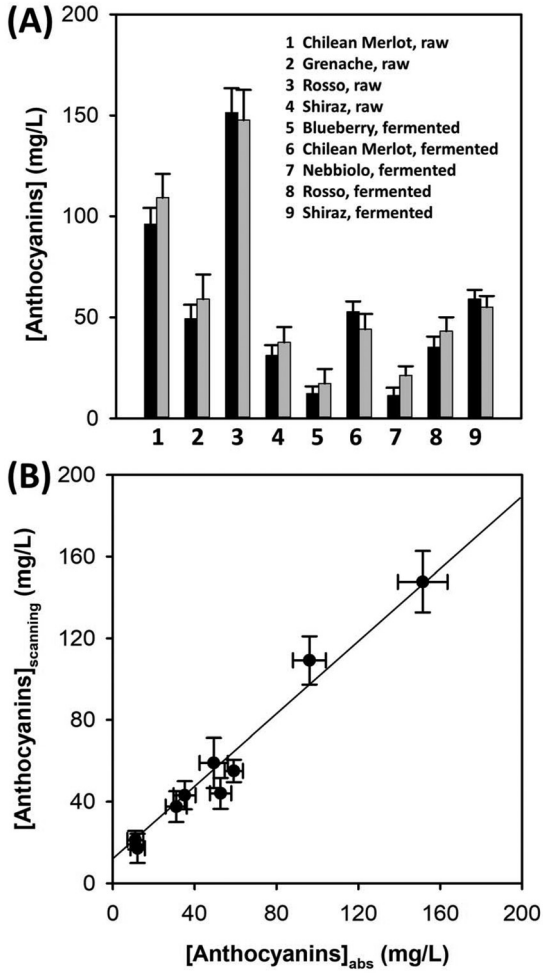

Fig. 5 (A) Comparison of the anthocyanin detection results using UV-vis spectrophotometry (black bars) and the Wi-Fi scanning method (gray bars). (B) Correlation between the anthocyanin concentrations determined *via* spectrophotometry ($[anthocyanins]_{abs}$) and the Wi-Fi scanning method ($[anthocyanins]_{scanning}$). The solid line in (B) is the best linear regression curve. The error bars in (A) and (B) were obtained from at least three replicated experiments.

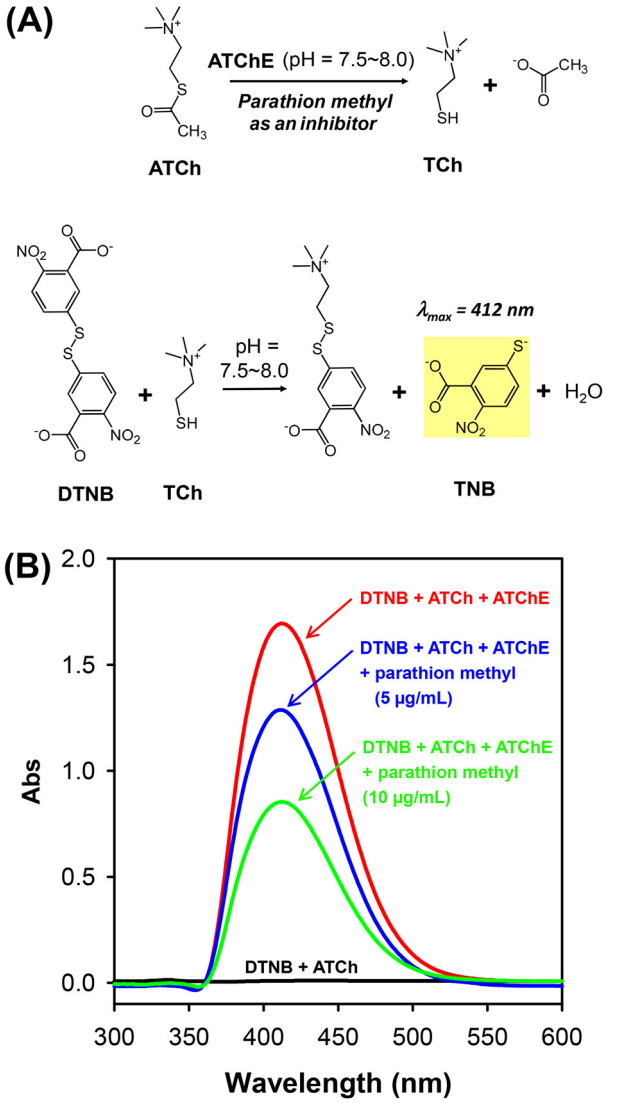

Fig. 6 (A) Reactions involved in the Ellman's assay for the colorimetric detection of parathion methyl. (B) UV-vis spectra recorded at 30 min of Ellman's assay solutions using 3 mM ATCh, 6 mM DTNB and 0.07 μg mL^{-1} AChE. The solution is pre-incubated together with 0 μg mL^{-1} (red curve), 5 μg mL^{-1} (blue curve) and 20 μg mL^{-1} parathion methyl (green curve). The black curve is the UV-vis spectrum of 3 mM ATCh and 6 mM DTNB only (no AChE added).

AChE, ATCh and DTNB, the reaction time was kept at 20 min) results in a strong absorption band (red curve) with the peak wavelength at 412 nm; upon pre-incubating AChE with 5 μg mL^{-1} parathion-methyl, the absorption peak decreases significantly (blue curve), and a further decrease is observed when the concentration of parathion methyl was increased to 20 μg mL^{-1} (green curve). As a control, no adsorption peak was observed when AChE was not added to Ellman's assay (only ATCh and DTNB, black curve).

Similar to the procedure depicted in Fig. 3, to perform Ellman's assay on hydrogel-paper disk arrays, the "empty" disk is pre-loaded with 20 μL of a solution of ATCh and DTNB mixture (1.0 mg mL^{-1} and 2.5 mg mL^{-1} respectively, dissolved in PB buffer, pH = 7.5). After that, 20 μL solution of AChE (pre-incubated with different concentrations of parathion methyl at 37 °C for 1 h in PB buffer, pH = 7.5) was added to each of the assay disk, followed by monitoring the color change and Wi-Fi scanning to obtain the results.

In contrast to the anthocyanin colorimetric detection, for which the color changes immediately like a pH indicator,[39] the colorimetric detection of parathion methyl depends on an enzymatic reaction and produces a "signal-off" response. Thus, both the enzyme concentration and the assay time play important roles in the assay performance. For AChE used in Ellman's assay, if its concentration were too high, higher concentrations of parathion methyl would be needed to inhibit its activity and lead to poor sensitivity; if the AChE concentration were too low, the blank color signal (no incubation with para-

thion methyl) could be too weak or take too long to reach a satisfactory color intensity. With an optimized ATChE concentration, the assay time needs to be carefully adjusted since the color could be weak if the reaction time is too short, or the color could become saturated if the reaction time is too long. In this study, we systematically optimized these factors, and the best assay performance was achieved with 0.25 μg mL^{-1} ATChE and a reaction time of 25 min. The details of optimization experiments are provided in the SI (Fig. S8–S11).

Under the optimized conditions, we performed Ellman's assay using the Wi-Fi scanning method after incubating ATChE with different concentrations of parathion methyl (0–20 μg mL^{-1}). Fig. 7(A) shows the scanned image of the detection results (three repeats in a 4 × 15 array format). It is clear to see that the higher concentration of parathion methyl leads to attenuated yellow intensity as a result of its inhibition effect on the ATChE activity. By analyzing the color intensities at each assay disk, the normalized yellow intensity ($Y/\sum$CMYK × 100%, $\sum$CMYK = C + M + Y + K) as the sensing response was plotted against the concentration of parathion methyl to generate the calibration curve. As shown in Fig. 7B, the normalized yellow intensity decreases monotonically before reaching a plateau at around 10 μg mL^{-1}; moreover, a linear response was found from 0 to 6 μg mL^{-1} (R^2 > 0.99). Fig. 7C is the calibration data obtained using conventional UV-vis spectrophotometry measurements (performing Ellman's assay in a microplate and using a plate reader to measure the absorbance), which has a similar "saturation" level (>10 μg mL^{-1}) and a linear response range (0–6 μg mL^{-1}). More importantly, the LOD values of parathion methyl determined from the two linear regression fits in Fig. 7B and C are close to each other, *i.e.*, 0.34 ± 0.12 μg mL^{-1} and 0.25 ± 0.10 μg mL^{-1}, respectively, indicating that the sensing performance of the two methods are very similar. Such a sensing performance is better than the quantitative results obtained *via* smartphone imaging in terms of both LOD and R^2 value of the linear fit (Fig. S14 in the SI) and comparable to previously reported colorimetric sensors based on Ellman's assay for the quantitation of parathion methyl, for which the LODs are from ng mL^{-1} to μg mL^{-1}.[49,50]

To further compare the sensing performance, drinking water (tap water) spiked with two different concentrations of parathion methyl (0, 2.0 and 5.0 μg mL^{-1}) was tested by quantifying the results of Ellman's assay with those of UV-vis spectrophotometry and the Wi-Fi scanning method. As presented in Table 1, the determined concentrations of parathion methyl ($[\text{parathion methyl}]_{\text{abs}}$ and $[\text{parathion methyl}]_{\text{scanning}}$) are both close to the spiked concentration of parathion methyl, *i.e.*, $[\text{parathion methyl}]_{\text{added}}$, with satisfactory recovery rates (between 90 and 109%). Remarkably, it was found that after six months of storage under ambient conditions (room temperature), the hydrogel-paper disks still exhibit similar sensing performance (Fig. S16 in the SI).

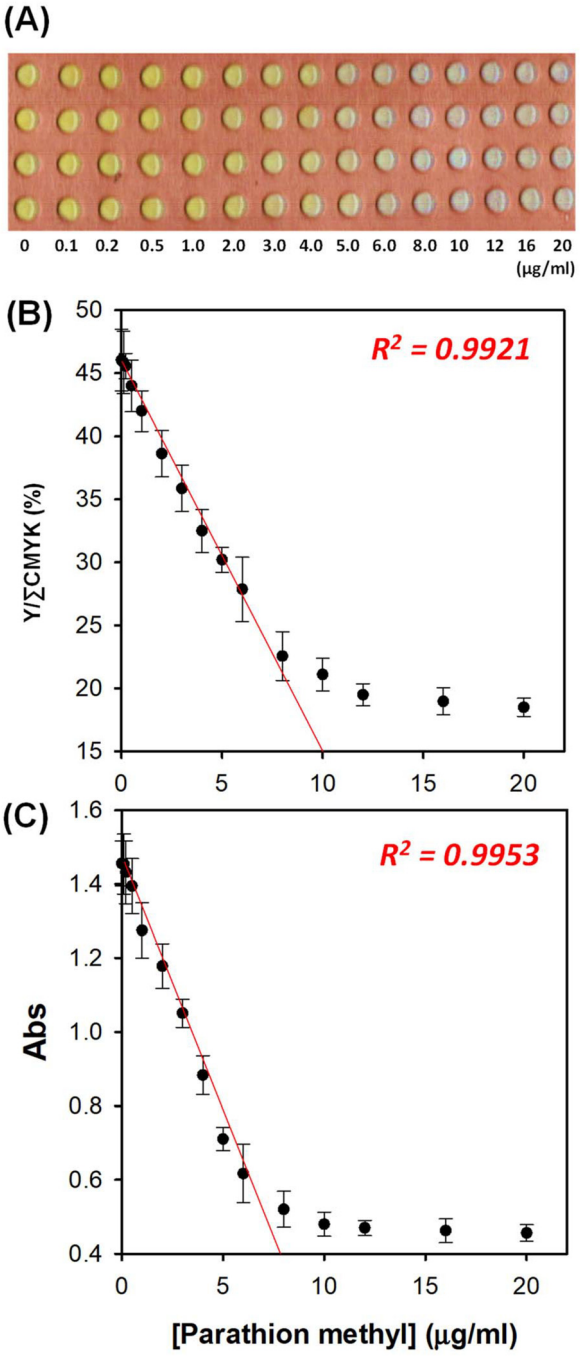

Fig. 7 (A) Wi-Fi scanned image of Ellman's assay performed on hydrogel/paper disks (three repeats in a 4 × 15 array) for the detection of parathion methyl (0–20 μg mL^{-1}). (B) Dependence of normalized *Y* value ($Y/\sum$CMYK) on the concentration of parathion methyl; the red solid line shows the best linear fit to the experimental data up to 6 μg mL^{-1}. (C) UV-vis absorbance measurements of Ellman's assay solutions in the presence of 0 to 20 μg mL^{-1} of parathion methyl. The red line is also the best linear fit to the data from 0 to 6 μg mL^{-1}. The error bars in (B) and (C) were obtained from four repeated experiments.

2.4. Comparison with other portable analytical systems and future perspectives

Nowadays, smartphones have become a popular imaging tool for colorimetric assays due to their intriguing advantages as described in the Introduction section. However, the color information accuracy of smartphone images is often limited by several factors.[21,51] The most critical factor is uncontrolled

Table 1 Detection results of spiked parathion methyl in drinking water with Wi-Fi scanning and UV-vis spectrophotometry methods

$[\text{Parathion methyl}]_{\text{added}}$ (μg mL^{-1})	$[\text{Parathion methyl}]_{\text{abs}}$ (μg mL^{-1})	$[\text{Parathion methyl}]_{\text{scanning}}$ (μg mL^{-1})
0.0	Not detected	Not detected
2.0	1.89 ± 0.08 (90% to 99% [a])	2.07 ± 0.11 (98% to 109% [a])
5.0	5.15 ± 0.12 (101% to 106% [a])	4.91 ± 0.19 (94% to 102% [a])

[a] Recovery rates (100% × $[\text{parathion methyl}]_{\text{determined}}$)/($[\text{parathion methyl}]_{\text{added}}$).

illumination, as variations in surrounding light or the use of flash can cause glare, shadows, and uneven brightness, thereby compromising the accuracy of color analysis.[51,52] Perspective distortion is another factor of limitation, particularly when the objectives are not perfectly parallel or they have different focal distances to the camera lens.[16,53] To address these issues, a range of hardware accessories, including dark boxes, convex lenses, and 3D-printed camera holders, have been explored to standardize the imaging condition of smartphones and improve the color analysis accuracy.[16] In contrast, with a linear image sensor (typically a CCD or contact image sensor), a built-in uniform light source (LED) and a cover lid, flatbed scanners have highly reproducible imaging conditions; more importantly, the images obtained using scanners are not affected by ambient lights and perspective distortion (fixed focal distance across the entire scan area), which results in more consistent resolution and highly accurate color information across the entire image. Besides the conventional office scanner, the commercially available handheld Wi-Fi scanners further promoted their use as superior alternatives to smartphones for reading PON tests (performing on-site colorimetric assays).

Compared to our previous study, where the anthocyanin pre-loaded hydrogel-paper disks were assembled onto a hydrophobic substrate (achieved by pre-treatment with 0.2% OTS/hexane solution) and merely used as a pH test strip,[34] the hydrogel-paper disk array developed in this work exhibits significant improvements and advantages. Firstly, the preparation of blank hydrogel/paper disks not only simplifies the fabrication process but also allows for much broader applications (can be loaded with any colorimetric reagents, and they are applicable for both enzymatic and chemical assays). Moreover, by simply assembling the paper disks on a commercial hydrophobic tape (no additional surface modification steps), a detection array of desired patterns and a number of reaction zones can be readily obtained; the long shelf-life (>6 months) also makes it possible for large-scale production and to be used as an economic alternative to conventional microplates for multiplex and high-throughput colorimetric detection (the 4 × 15 array testing results shown in Fig. 7A are approching the testing capacity of a 96-well microplate). We have demonstrated that the quantitation results of this new portable analytical system (Wi-Fi scanning + hydrogel-paper disk array) are comparable to conventional spectrophotometric measurements and smartphone analysis, which augments its great potential for practical use. In addition, a web-based mobile app (ChromaDetect) was developed in this study, which allows robust and convenient quantitative color analysis using smartphones, pads, and laptops compared to conventional software analysis using only computers (*e.g.*, photoshop or Image J).

It should be noted that for practical application, the sample volume could have a complex impact on the hydrogel-filter paper sensing platform (*e.g.*, it directly controls the amounts of reagents/analytes used for each detection, evaporation could lead to dramatically increased local concentrations of colorimetric reagents, the enzyme activity could be limited if the diffusion or capillary flow is too slow, and insufficient or excess volume may result in uneven reagent distribution or a "coffee ring" effect), which should be optimized for specific colorimetric assays by considering both technical and economic factors.

By and large, we expect such a digitized, Wi-Fi scanning platform could be expanded to a broad range of colorimetric assays, such as nanoparticle based colorimetric assays and colorimetric immunoassays (with nanoparticles, labelled bio-recognition elements or substrates as pre-loading reagents). In addition to agarose films, the performance of this new platform when applied to specific colorimetric assays could be further enhanced by investigating the most suitable hydrogel material (alginate, chitosan, gelatin, *etc*.). The quality of scanned images can be further improved with a less curved objective (*e.g.*, smaller liquid volume), an adjustable device to minimize the scanning space above the liquid drop, and more advanced portable scanners with higher resolution or intelligent scanning options (*e.g.*, multi-direction and multi-mode scanning).

It is also anticipated to convert this portable, low-cost, user-friendly platform into commercially available PON devices, which will provide an alternative to laboratory-based spectroscopic methods and greatly enhance the accessibility of quantitative colorimetric analysis in resource-limited settings or remote areas. Its robustness, scalability and ease of use will not only advance the analytical sciences (*e.g.*, facilitating rapid field testing, environmental monitoring, and on-site diagnostics) but also generate broad societal benefits by supporting public health, food safety, and environmental protection initiatives. To achieve this goal, the long-term stability of the hydrogel-paper disk array (with or without preloaded colorimetric reagents) will also be evaluated (which is, underway or being planned in our laboratory).

3. Conclusion

In this study, we have developed a portable PON platform that allows multiplexed, convenient, and quantitative analysis by using a disposable detection array made of hydrogel/filter paper mini-disks, a handheld Wi-Fi scanner to capture the resulting image, and a customized app for analyzing the color information (based on either RGB or CMYK color space). Its performance has been thoroughly validated with two colorimetric assays: the pH-differential colorimetric assay for anthocyanin and Ellman's assay for parathion methyl. It was demonstrated that the quantitation results (*e.g.*, response ranges, LODs, and real sample detection) obtained with the Wi-Fi scanning platform are comparable to those using conventional spectrophotometric measurements, indicating its reliability and feasibility for practical applications (either on-site chemical analysis or point-of-care medical diagnosis).

4. Experimental section

4.1 Materials and reagents

Agarose (low-EEO/multi-purpose, molecular biology grade, Fisher BioReagents), HCl (37%, USLI grade, GEM Microelectronic Materials, Nevada, AZ), NaOH (beads, ≥97.0%, ACS, VWR Chemicals BDH), cyanidin 3-*O*-glucoside chloride (Cy3G) standard (98% HPLC purity, Aobious Inc., Gloucester, MA), parathion methyl (analytical standard, Sigma-Aldrich, St Louis, MO), acetylcholine chloride (ATCh, ≥99% TLC, Sigma-Aldrich, St Louis, MO), 5,5′-dithio-bis-(2-nitrobenzoic acid) (DTNB, ≥98%, Sigma-Aldrich, St Louis, MO), acetylcholinesterase (ATChE, Sigma-Aldrich, St Louis, MO), glycerol (ACS reagent ≥99.5%, Sigma-Aldrich, St Louis, MO), ethanol (95%, Commercial Alcohols, Toronto, ON), disodium hydrogen phosphate heptahydrate ($Na_2HPO_4{\cdot}7H_2O$, Caledon Laboratories Ltd, Georgetown, ON), sodium dihydrogen phosphate monohydrate ($NaH_2PO_4{\cdot}H_2O$, Caledon Laboratories Ltd, Georgetown, ON), sodium acetate (CH_3COONa, ACS reagent ≥99.0%, Sigma-Aldrich, St Louis, MO) and acetic acid (CH_3COOH, ≥99.0%, Sigma-Aldrich, St Louis, MO) were used as received unless otherwise noted. All beverage samples were provided by Laca Biotech Inc. and tested as received (except for dilution when needed). Deionized water (18.2 MΩ cm^{-1}) used throughout all experiments to prepare standard solutions and samples was produced fresh using a Barnstead EasyPure UV/UF compact water system (Dubuque, IA). Double-sided tape was purchased from Intertape Polymer Group. Grade-3 filter paper was obtained from Cytiva (Marlborough, MA).

Anthocyanin (Cy3G) stock solution: 1.0 mg mL^{-1} stock solution of Cy3G was prepared with DI water and stored at 4 °C before use. Acetylcholinesterase (ATChE) stock solution: 1.0 mg mL^{-1} stock solution (10 μL aliquots to avoid freeze–thaw cycles) was prepared by using sterile (*via* 0.2 μm filter) 0.1 M PB buffer containing 10% glycerol; the aliquots were stored at −20 °C before use. Parathion methyl stock solution: 1.0 mg mL^{-1} stock solution was prepared with ethanol and stored at 4 °C. Buffer solutions: pH 1.0 solution was prepared with 1.0 M HCl, pH 4.5 buffer was prepared with CH_3COONa and CH_3COOH (adjusted with 0.1 M HCl or 0.1 M NaOH), and pH 7.5 PB buffer (0.1 and 0.01 M) was prepared with $NaH_2PO_4{\cdot}H_2O$ and $Na_2HPO_4{\cdot}7H_2O$ (pH adjusted with 0.1 M HCl or 0.1 M NaOH).

4.2. Fabrication of hydrogel-paper disk assay

The hydrogel-coated filter paper was prepared by dissolving agarose powder in 70 °C water (w/v = 5%) and stirred for at least 15 min to obtain a clear, homogeneous solution (all agarose dissolved).[34] Then, the agarose solution was immediately poured onto a piece of grade-3 filter paper placed inside the lid of a plastic Petri dish, and the bottom of the Petri dish was pressed on top. To control the thickness of the agarose film, double-sided tapes were positioned between the dish bottom and lid to separate them by ∼0.75 mm. After pressing for at least 30 min, the hydrogel-coated filter paper was taken out, dried overnight, and was stored at room temperature before use.

To assemble the mini-disk array, the hydrogel-coated filter paper was cut into 5 mm diameter disks by using an Explore 4 smart cutting machine (Cricut, Inc., South Jordan, UT). The paper disks were then aligned and stuck to double-sided tape (the other side of the tape was attached to a solid support substrate) with an appropriate distance between each other (>0.5 cm).

4.3. Colorimetric assay procedures for anthocyanin and parathion methyl

Anthocyanin (Cy3G) detection (Wi-Fi scanning). 20 μL of the pH 1.0 solution or pH 4.5 buffer was loaded on the hydrogel-paper disk array, dried overnight, and stored in an ambient environment before use. For the quantitation, 20 μL of Cy3G solution of different concentrations (diluted from the 1.0 mg mL^{-1} stock solution with water, from 0 to 120 mg L^{-1}) was added to the pH 1.0 solution and the pH 4.5 buffer pre-loaded on the disk. After observing the color change, a mini-handheld iScan portable scanner (Brand: Loomza) was used to capture the images of detection results (JPG format), followed by quantitative analysis with the customized app (to determine the normalized *R* value) and construct the calibration curve.

Anthocyanin (Cy3G) detection (UV-vis). The 1.0 mg mL^{-1} stock solution of Cy3G was diluted to different concentrations (0 to 200 μg mL^{-1}) with the pH 1.0 solution and the pH 4.5 buffer. For each diluted Cy3G solution, 1.0 mL was transferred to a quartz cuvette and its spectrum was collected using an Ocean Optics QE65000 spectrophotometer equipped with a DU-2000-BAL deuterium and tungsten lamp and a 600 μm SR optical fiber probe (Winter Park, FL). The absorbance at the maximum wavelength of each diluted Cy3G solution (512 nm) was quantitatively analyzed using the pH differential method.

Parathion methyl detection (Wi-Fi scanning). 20 μL of the solution mixture of ATCh (2.5 mg mL^{-1}) and DTNB (1.0 mg mL^{-1}) was loaded on the hydrogel-paper disk array, dried overnight, and stored in an ambient environment before use. For

parathion methyl detection, the 1.0 mg mL^{-1} stock solution was diluted with 10 mM PB buffer to desired concentrations (0–50 μg mL^{-1}). For the AChE inhibition assay, 1 μL of AChE aliquot (1 mg mL^{-1}, stored at −20 °C) was first diluted with 10 mM PBS buffer to 150 μL; subsequently, 4 μL of diluted AChE was added to 100 μL of parathion methyl of different concentrations and incubated at 37 °C for 30 min (the final AChE concentration is 250 ng mL^{-1}). Then, 20 μL of incubation solution was added to the ATCh/DTNB preloaded disk; after waiting for 25 min, we used the handheld Wi-Fi scanner (iScan) to capture the assay image, followed by quantitative analysis with the app (to determine normalized *Y* values).

Parathion methyl detection (UV-vis). 1.0 mg mL^{-1} parathion methyl stock solution was diluted with 10 mM PB buffer to desired concentrations (0–50 μg mL^{-1}). For AChE inhibition, 1 μL of AChE aliquot (1 mg mL^{-1}, stored at −20 °C) was first diluted using the PB buffer to 150 μL; subsequently, 4 μL of the diluted AChE was added to 200 μL of parathion methyl of different concentrations and incubated at 37 °C for 30 min (the final AChE concentration is 0.1 μg mL^{-1}). After incubation, 20 μL of the binary solution of ATCh (2.5 mg mL^{-1}) and DTNB (1.0 mg mL^{-1}) was added, and after waiting for 25 min, the absorbance was measured. To obtain the spectrum and determine the absorbance peak wavelength, the solution was transferred to a cuvette and scanned with the same spectrophotometer noted above. For the quantitative detection, each incubation solution was prepared in a well on a Fisher microplate (Fisher Scientific, Hampton, NH); after adding the ATCh/DTNB mixture, a Tecan Infinite 200 Pro microplate reader (Männedorf, Switzerland) was used to measure the absorbance at the peak wavelength (412 nm).

Conflicts of interest

There are no conflicts to declare.

Data availability

The authors confirm that the data supporting the findings of this study are available within the article and its supplementary information (SI). Supplementary information: description of the design and function of the color analysis app; the fabrication and detection procedure of hydrogel-coated filter paper; the influence of using a scanning box on the imaging results; optimization of the two colorimetric assays performed using the Wi-Fi scanning method and conventional UV/vis spectrophotometric measurements; additional photos and quantitation results of real samples; the original codes for the ChromaDetect app. See DOI: https://doi.org/10.1039/d6an00255b.

Acknowledgements

This work was funded by the Natural Science and Engineering Research Council (NSERC) of Canada through a Discovery Grant (PI: H. Y.) and an Alliance International Catalyst Grant (PIs: H. Y. and A. T.). This work also made use of the 4D LABS shared facilities supported by the Canada Foundation for Innovation (CFI), British Columbia Knowledge Development Fund (BCKDF), Western Economic Diversification Canada (WD) and Simon Fraser University (SFU). P. P. would like to thank the Government of Canada for the SEED (Scholarships and Educational Exchanges for Development) scholarship, which supported his stay at SFU as a visiting graduate student. We also thank Shirin Yazdani for her help in preparing some of the procedure diagrams in the SI.

References

1 Z. Jin, W. Yim, M. Retout, E. Housel, W. Zhong, J. Zhou, M. S. Strano and J. V. Jokerst, *Chem. Soc. Rev.*, 2024, **53**, 7681–7741.
2 C. V. Sapan, R. L. Lundblad and N. C. Price, *Biotechnol. Appl. Biochem.*, 1999, **29**, 99–108.
3 Y. Wu, J. Feng, G. Hu, E. Zhang and H.-H. Yu, *Sensors*, 2023, **23**, 2749.
4 Y. K. Shrestha and S. K. Shrestha, in *Advances in Colorimetry*, IntechOpen, 2023.
5 J. Yang, X. Wang, Y. Sun, B. Chen, F. Hu, C. Guo and T. Yang, *Biosensors*, 2022, **13**, 29.
6 W. Zhao, M. A. Brook and Y. Li, *ChemBioChem*, 2008, **9**, 2363–2371.
7 Y. Lee, I. Haizan, S. B. Sim and J.-H. Choi, *Biosensors*, 2025, **15**, 362.
8 Y. Song, W. Wei and X. Qu, *Adv. Mater.*, 2011, **23**, 4215–4236.
9 A. P. Vijaya Kumar Saroja, P. Joseph, K. Daniel, S. Lakshmanan, T. Kinoshita and S. Muthusamy, *Mater. Sci. Eng., C*, 2017, **78**, 1231–1245.
10 A. Ko and C. Liao, *Anal. Methods*, 2023, **15**, 4377–4404.
11 F. Di Nardo, M. Chiarello, S. Cavalera, C. Baggiani and L. Anfossi, *Sensors*, 2021, **21**, 5185.
12 W. C. Mak, V. Beni and A. P. F. Turner, *TrAC, Trends Anal. Chem.*, 2016, **79**, 297–305.
13 V. Kumar and K. D. Gill, in *Basic Concepts in Clinical Biochemistry: A Practical Guide*, Springer, 2018, pp. 17–20.
14 G. A. Parker and D. Boltz, in *Modern Methods of Geochemical Analysis*, Springer, 1971, pp. 97–126.
15 B. R. Sun, A. G. Zhou, X. Li and H.-Z. Yu, *ACS Sens.*, 2021, **6**, 1731–1744.
16 R. Deng, X. Chao, H. Li, X. Li, Z. Yang and H.-Z. Yu, *Analyst*, 2023, **148**, 735–741.
17 X. Li, F. Yang, J. X. Wong and H.-Z. Yu, *Anal. Chem.*, 2017, **89**, 8908–8916.
18 J. Guo, J. X. Wong, C. Cui, X. Li and H.-Z. Yu, *Analyst*, 2015, **140**, 5518–5525.
19 Y. Fan, J. Li, Y. Guo, L. Xie and G. Zhang, *Measurement*, 2021, **171**, 108829.

20 A. Roda, E. Michelini, M. Zangheri, M. Di Fusco, D. Calabria and P. Simoni, *TrAC, Trends Anal. Chem.*, 2016, **79**, 317–325.
21 D. V. Baker, J. Bernal-Escalante, C. Traaseth, Y. Wang, M. V. Tran, S. Keenan and W. R. Algar, *Lab Chip*, 2025, **25**, 884–955.
22 S. Qian, Y. Cui, Z. Cai and L. Li, *Biosens. Bioelectron.*, 2022, **11**, 100173.
23 S. Kanchi, M. I. Sabela, P. S. Mdluli and K. Bisetty, *Biosens. Bioelectron.*, 2018, **102**, 136–149.
24 L. Shen, J. A. Hagen and I. Papautsky, *Lab Chip*, 2012, **12**, 4240–4243.
25 J. Li, M. L. O'Neill, C. Pattison, J. H. Zhou, J. M. Ito, C. S. Wong, H.-Z. Yu and N. Merbouh, *J. Chem. Educ.*, 2023, **100**, 1234–1242.
26 J. Wang, L. Zhang, X. Li, X. Zhang and H.-Z. Yu, *RSC Adv.*, 2019, **9**, 23267–23275.
27 J. R. Askim and K. S. Suslick, *Anal. Chem.*, 2015, **87**, 7810–7816.
28 G. Sriram, M. P. Bhat, P. Patil, U. T. Uthappa, H.-Y. Jung, T. Altalhi, T. Kumeria, T. M. Aminabhavi, R. K. Pai and M. D. Kurkuri, *TrAC, Trends Anal. Chem.*, 2017, **93**, 212–227.
29 T. Kant, K. Shrivas, A. Tejwani, K. Tandey, A. Sharma and S. Gupta, *Nanoscale*, 2023, **15**, 19016–19038.
30 M. C. Carneiro, L. R. Rodrigues, F. T. Moreira and M. G. F. Sales, *Sensors*, 2022, **22**, 3221.
31 K. Fan, X. Wang, H. Gao, G. Han, L. Zhou and S. Fang, *Anal. Methods*, 2020, **12**, 1561–1566.
32 T. Choleva, C. Matiaki and D. L. Giokas, *Sens. Actuators, B*, 2023, **386**, 133729.
33 L. Zhang, H. Kwok, X. Li and H.-Z. Yu, *ACS Appl. Mater. Interfaces*, 2017, **9**, 39728–39735.
34 M. Leung, L. Zhang, X. Li and H.-Z. Yu, *Anal. Chem.*, 2024, **96**, 15808–15815.
35 V. J. Liebich, O. Avrutina, J. Habermann, L. M. Hillscher, M. Langhans, T. Meckel, M. Biesalski and H. Kolmar, *Biomacromolecules*, 2021, **22**, 2954–2962.
36 J. Tavakoli and Y. Tang, *Polymers*, 2017, **9**, 364.
37 W. Cheng, X. Wu, Y. Zhang, D. Wu, L. Meng, Y. Chen and X. Tang, *Trends Food Sci. Technol.*, 2022, **129**, 244–257.
38 S. Huang, G. Wang, H. Lin, Y. Xiong, X. Liu and H. Li, *Sens. Actuators Rep.*, 2021, **3**, 100049.
39 https://www.bhphotovideo.com/lit_files/255716.pdf, accessed March 4, 2026.
40 R. Mattioli, A. Francioso, L. Mosca and P. Silva, *Molecules*, 2020, **25**, 3809.
41 E. Sondheimer and Z. Kertesz, *Anal. Chem.*, 1948, **20**, 245–248.
42 J. Lee, R. W. Durst and R. E. Wrolstad, *J. AOAC Int.*, 2005, **88**, 1269–1278.
43 B. Fallico, E. Arena, E. Chiappara and G. Ballistreri, *Food Addit. Contam.*, 2010, **27**, 201–211.
44 F. L. Edwards and P. B. Tchounwou, *Int. J. Environ. Res. Public Health*, 2005, **2**, 430–441.
45 S. Garcia, A. Abu-Qare, W. Meeker-O'Connell, A. Borton and M. Abou-Donia, *J. Toxicol. Environ. Health, Part B*, 2003, **6**, 185–210.
46 P. S. Jaglan, R. B. March, T. R. Fukuto and F. A. Gunther, *J. Agric. Food Chem.*, 1970, **18**, 809–813.
47 I. S. Che Sulaiman, B. Chieng, M. Osman, K. Ong, J. Rashid, W. M. Wan Yunus, S. Noor, N. Kasim, N. Halim and A. Mohamad, *Microchim. Acta*, 2020, **187**, 131.
48 F. Worek, P. Eyer and H. Thiermann, *Drug Test. Anal.*, 2012, **4**, 282–291.
49 M. Bhattu, M. Verma and D. Kathuria, *Anal. Methods*, 2021, **13**, 4390–4428.
50 X. Meng, C. W. Schultz, C. Cui, X. Li and H.-Z. Yu, *Sens. Actuators, B*, 2015, **215**, 577–583.
51 X. Bao, S. Jiang, Y. Wang, M. Yu and J. Han, *Analyst*, 2018, **143**, 1387–1395.
52 S. Dutta, *TrAC, Trends Anal. Chem.*, 2019, **110**, 393–400.
53 G. Zhang, S. Song, J. Panescu, N. Shapiro, K. C. Dannemiller and R. Qin, *PLoS One*, 2023, **18**, e0287099.